Biomed Microdevices (2012) 14:669–677
DOI 10.1007/s10544-012-9647-6

A high-flux isopore micro-fabricated membrane for effective concentration and recovering of waterborne pathogens

Majid Ebrahimi Warkiani · Chao-Ping Lou · Hao-Bing Liu · Hai-Qing Gong

Published online: 24 March 2012

Abstract A high-flux metallic micro/nano-filtration membrane has been fabricated and validated for isolation of waterborne pathogens from drinking water. Obtained membrane with smooth surface and perfectly ordered pores was achieved by a high yield and cost effective multilevel lithography and electroplating technique. The micro-fabricated membrane was also strengthened with an integrated back-support, which can withstand a high pressure during filtration. The results of microfiltration tests with model particles revealed the superior performance of the micro-fabricated filter than current commercial filters in sample throughput, recovery ratio, and reusability. This study highlighted the potential application of micro-fabricated filer in rapid filtration and recovery of *C. parvum* oocysts for downstream analysis.

Keywords Micro-fabricated membrane · Lithography · Fouling · Pathogen · Microfiltration

1 Introduction

Many problems associated with the physical, chemical, and microbiological studies of the human environment require rapid concentration of small particles suspended in minute concentration within the two foremost environmental vehicles which human involve continuously in large quantities—namely, air and water (Baker 2004; Beyor et al. 2008). Waterborne pathogens like *Cryptosporidium parvum* and *Giardia* that exist in rivers and lakes can cause intestinal illnesses. Infections by these parasites can cause acute gastrointestinal symptoms in normally healthy people, and can lead to life-threatening conditions in individuals with impaired immune systems, such as patients with acquired immune deficiency syndrome (Ahmad et al. 2011; Zourob et al. 2008). Filtration based methods have been used widely for isolation and recovery of *Cryptosporidium parvum* and *Giardia* (oo)cysts over the past decades (Noble 1995; Zarlenga and Trout 2004). Many membrane filtration techniques have been developed and employed to quantify the presence of these parasites in surface and treated water samples, including polycarbonate track-etched membrane filter (Lee et al. 2004), compressed-foam depth filters (Wohlsen et al. 2004), and yarn-wound cartridge filters (Nieminski et al. 1995). Efficiency assessment of these membranes has shown various degrees of recovery for *Giardia* and/or *Cryptosporidium* (Lee et al. 2004; Wohlsen et al. 2004; Karim et al. 2010). The major drawbacks which normally lead to poor cell recovery in current techniques are mainly associated to the structure of these filters. Depth filters like cellulose, yarn-wound and glass fiber, which normally made of a thick bed of fiber or other materials, capture target cells (i.e. (oo) cysts) with some other bigger particles because their pore diameter is an average value in a certain scale range. Therefore, it is often difficult to realize an absolute separation and a full collection of (oo)cysts using these filters. In addition, it is normally required to apply a high transmembrane pressure (TMP) to facilitate flow through the depth filters due to their high thickness and tortuous pore path (Noble 1995; Zeman and Zydney 1996). Screen type filters like track-etched membrane (i.e. used in many U.S. Environmental Protection Agency (USEPA) recommended filters like Envirochek HV and

M. E. Warkiani · C.-P. Lou · H.-B. Liu · H.-Q. Gong (✉)
School of Mechanical and Aerospace Engineering,
Nanyang Technological University,
50 Nanyang Avenue,
Singapore 639798, Singapore
e-mail: mhqgong@ntu.edu.sg

CrypTest) (Karim et al. 2010; Leonard 2003; Clancy et al. 1999) are another well-known type of filters that employs relatively thin filter membranes in contrast to the depth filters. Although they have nominal pore sizes and have been used in a wide variety of industrial and medical applications, they tend to have a limited porosity (i.e. ≈ 5–10 %) (Ramachandran and Fogler 1999), which normally lead to a small throughputs due to the blockage on the surface of membrane. Moreover, track-etched membrane can just be made with circular pores; therefore, they are unsuitable for discriminating based on non-circular particle shape (Van Rijn 2004).

Hence, it is important to develop a micro/nano-filter with a smooth surface, identical pore-diameter, and high porosity for rapid separation and concentration of (oo)cysts according to their dimensions from potable water. Recent developments in MEMS technology have provided novel techniques for controlling the detailed microstructure of membrane materials, allowing the fabrication of membranes with precise pore size and shape (Van Rijn 2004). In recent years, different methods have been proposed to create membranes with cylindrical pores like conventional/interference lithography and silicon etching technology (Kuiper et al. 1998; Warkiani et al. 2011a, b), nanoimprinting using alumina template (Yanagishita et al. 2007), phase separation micromolding (Gironès et al. 2006), and dissolving mold techniques (Chen et al. 2010). Regardless of capability of these methods for fabrication of organic/inorganic microsieve with pore size down to hundred nanometers, some major impediments like complexity and cost of the fabrication process as well as difficulty for large-scale production are associated with these techniques (Van Rijn 2004).

In all the emerging membrane technology, transition to commercial success requires an economical process with precise control over device performance as well as scalability of the fabrication process (Stroeve and Ileri 2011). In this study, we demonstrate a high-yield and low cost process for fabrication of high-flux metallic micro/nano-filters using conventional lithography and electroplating techniques. This process is similar to the LIGA process which widely used in industry for precision manufacturing of high-aspect-ratio micro-components such as micro-fluidic chips and optical fiber connectors (Van Rijn 2004; Malek and Saile 2004). Obtained membranes have extremely smooth surface, uniform pore size and high porosity, which can filter large volumes of tap-water in relatively short time periods. An integrated support layer with large openings also attached to the membranes to protect the membrane from tearing and failure during handling and filtration. Sample loading and back-flushing using micro-fabricated filter showed improved performance in sample throughput and recovery than existing commercial micro-filters for the same purpose. This research demonstrated the potential application of the high-flux micro/nano-fabricated filters in efficient monitoring of waterborne pathogen's contamination in the water-supply systems.

2 Design and fabrication

2.1 Fabrication of microfilter

Figure 1 shows schematically the fabrication process of metallic micro-fabricated membrane with integrated back-support. First, a thick standard 100 mm diameter, (1,0,0)-oriented silicon wafer, was cleaned carefully in piranha solution (96 % H_2SO_4 and 30 % H_2O_2) for 20 min at 120 °C to remove any organic contaminations on the wafer surface. After rinsing with DI water and drying with N_2 gas, the substrate was submerged in the buffered oxide etchant (BOE) for 5 min to clean the natural oxide layer. This step has a significant impact on adhesion of seed layer to the substrate. Then electrical contact was provided through a 300 nm thick Cr/Cu seed layer that was deposited on the silicon wafer by sputtering process, using a magnetron sputtering machine (Fig. 1(a)).

To aid the good adhesion of photo-resist to the seed layer, the dehydration bake-step was performed under vacuum in Suss machine (Delta 150 VPO) for 2 min. Afterward, a 10 μm thick AZ9260 (Microchemicals GmbH) photo-resist was spin-coated on the wafer at a spin speed of 2000 rpm (Fig. 1(b)). In order to avoid bubbles, the photo-resist was poured onto the substrate directly from a bottle with a large aperture. Soft baking process was performed on a carefully leveled hot plate at 110 °C for 4 min and followed by 2 min relaxation at 25 °C. After soft baking the AZ film on the hot plate, a chrome coated glass mask with rectangular features (3×8 μm) was used to transfer the patterns into the AZ photoresist. UV-Lithography was processed by Karl Suss MA6 mask aligner (Karl Suss Inc.) in the hard contact mode between the silicon wafer and the mask with a 350 W mercury lamp with a high pass UV filter in order to cut off undesired short wavelength (Fig. 1(c)). Finally, the exposed film was developed at room temperature in AZ 400 k (Microchemicals GmbH) developer, which was diluted with DI water (1:2) for 2 min with manual agitation (Fig. 1(d)). The width of pillars can be controlled precisely using the UV exposure and development time. After rinsing with DI water and drying with N_2 gas, the wafer was mounted in a holder that provides a homogeneous electric contact with the conducting layer coated on the substrate. Then, the holder was immersed in the electroplating bath to electroform the nickel between photo-resist pillars (Fig. 1(e)). The bath solution has a volume of about 5 l, which operates at 50 °C, and its composition is shown in Table 1.

Nickel sulphamate is the main source of nickel ions for electroforming that will be deposited in the cathode while nickel chloride promotes nickel anode dissolution and prevents anode passivation (i.e. causing pH increase and sulfamate hydrolysis, which leads to increase internal stress) (McGeough et al. 2001).

The Boric acid acts as a pH buffer that prevents basic nickel compound formation at the cathode and thereby minimizing

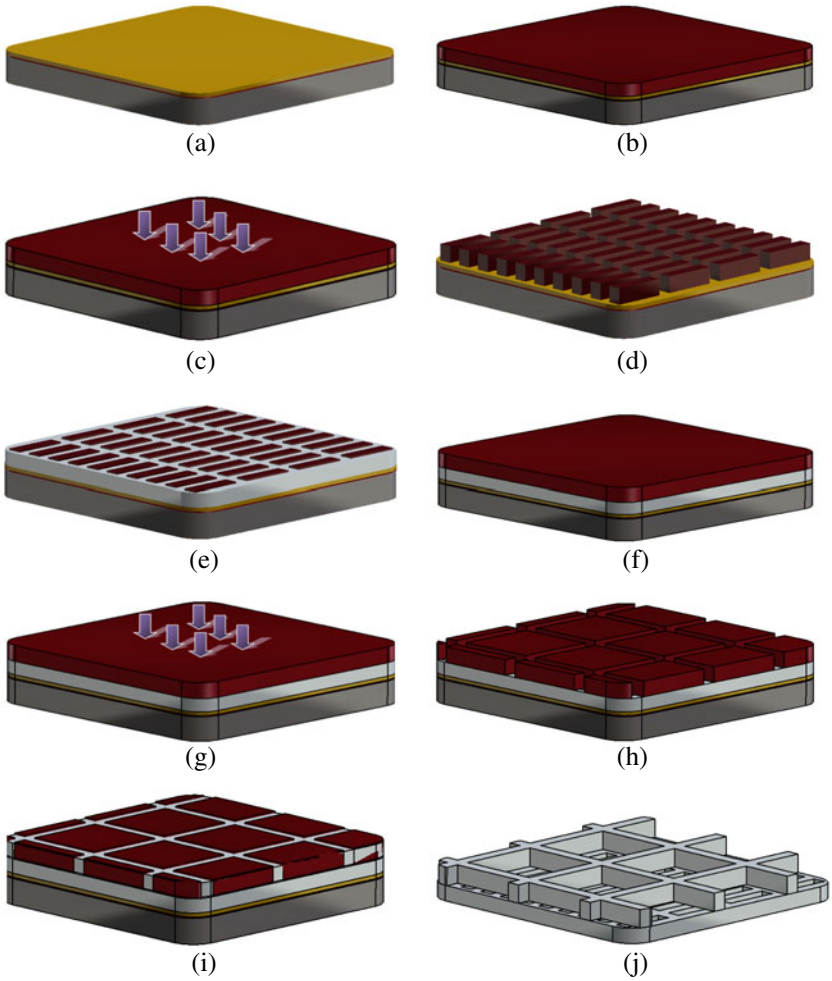

Fig. 1 Schematical illustration of the fabrication process, (**a**) deposition of seed layer (Cr/Cu) on a Si substrate, (**b**) spin-coating of a thick layer of AZ9260 on the Si wafer, (**c**) UV exposure through a quartz mask with rectangular-shape features, (**d**) development of the exposed film inside AZ developer, (**e**) electroplating of Ni between photo-resist pillars, (**f**) spin-coating of another thick layer of AZ9260, (**g**) UV exposure through a plastic mask with square-shape features, (**h**) development of the exposed film inside AZ developer, (**i**) second electroplating of Ni between photo-resist features, (**j**) releasing the through-hole membrane with integrated back-support by dissolving the photo-resist and seed layer in acetone and Cu etchant, respectively

the internal stress of the nickel deposits. Appropriate additives have been added to the bath solution in order to shift the stress from tensile to compressive, prevent pitting formation on the cathode surface and also adjust the pH value during operation (Spiro 1971).

2.2 Fabrication of back-support

The micro-fabricated membrane is too thin and may easily fold or break during filtration or handling. Hence, it is required to strengthen the membrane with a back-support with large apertures. For this purpose, a thick layer of AZ 9260 was again spin-coated on the membrane surface (Fig. 1(f)) and lithography was performed using a plastic mask with square shape features (600×600 μm) to transfer the pattern to the photo-resist (Fig. 1(g)). Then, the exposed film was developed at room temperature in AZ 400 k developer for 3 min followed by rinsing with DI water and N_2 gas drying (Fig. 1(h)). The second electroplating was performed in the same bath for around 15 min to form the support structure between the photo-resist gaps (Fig. 1(i)). Afterwards, photo-resists, which remain from the previous steps, were dissolved in an acetone bath. After washing the wafer with Isopropanol and also DI water, the seed layer was removed using Cu etchant (Sigma Aldrich) in order to release the micro-fabricated membrane from the substrate (Fig. 1(j)). Ultrasonic agitation can be useful in this step because it expedites the releasing process and also prevents from adhesion of the membrane to the substrate.

Table 1 Chemical composition of the Ni electrolyte bath

Chemical name	Formula	Bath concentration
Boric acid	H_3BO_3	30–50 (gr/l)
Nickel chloride	$NiCl_26H_2O$	5–20 (gr/l)
Nickel sulphamate	$Ni(NH_2SO_3)_2$	320–400 (gr/l)
Additives	N/A	5–20 ml/l

3 Result and discussion

By employing conventional UV-lithography and electroplating techniques, we present a low cost method for fabrication of high-flux micro/nano-filters with perfectly ordered pores

and integrated back-support. These techniques have been used widely in the semiconductor industry; therefore, this method can be scale-up for mass production of micro-fabricated membranes.

3.1 Membrane morphology

Figure 2(a) and (b) show the SEM photographs of the photo-resist pillars with the nickel thin film deposited between the gaps, respectively. The nickel film cannot be thicker than about 85–90 % of the photo-resist structures height; otherwise the nickel film will fill the microfilter pores. Thickness of electroplated nickel coating can be calculated from the Faraday's law (Spiro 1971). The obtained metallic membrane with slotted pores is also illustrated in Fig. 2(c) and (d).

It can be seen that array of rectangular pores (2.5×8 μm) perfectly formed. The width of photo-resist pillars was reduced from 3 to 2.5 μm precisely by controlling the exposure and development time during lithography. It should be noted that a slotted pore design provides a significantly lower pressure drop than a circular pore membrane because the membrane resistance is much smaller (Van Rijn 2004). In addition, it has been shown by other researchers that slotted pore membrane is less vulnerable to the particle bridging and therefore, fouling than the circular one (Chandler and Zydney 2006).

Figure 3 shows also an optical microscopic image of a 100 mm diameter metallic membrane on a silicon substrate. The close up view shows the SEM image of the integrated back-support formed on top of the membrane. As it discussed before, integrated back-support safeguards the membrane from tearing and failure during micro-filtration besides keeping it flat.

3.2 Membrane strength

Experimental and numerical investigations were carried out to calculate the mechanical stability of the metallic micro-fabricated membranes. Based on the following correlation which was introduced by Van Rijm group (Van Rijn et al. 1997), the mechanical strength of a perforated membrane depends on the thickness of membrane, the Young's modulus of membrane, the intrinsic tensile stress, and also distance between the bars of integrated back-support.

$$P_{\max} = 0.58 \frac{h\sigma_{yeff}{}^{3/2}}{lE_{eff}{}^{1/2}}$$

where P_{max} is the maximum load (i.e. bursting pressure), h is the membrane thickness, l is the distance between the back-support bars, E_{eff} and σ_{yeff} are the effective Young's modulus and yield strength, respectively. The membrane porosity in this model is considered by a factor $(1-K)$ for calculation of E_{eff} and σ_{yeff}, where K is the porosity. Based on this theory, a perforated membrane can be modeled as a non-perforated membrane with adjusted Young's modulus and yield strength.

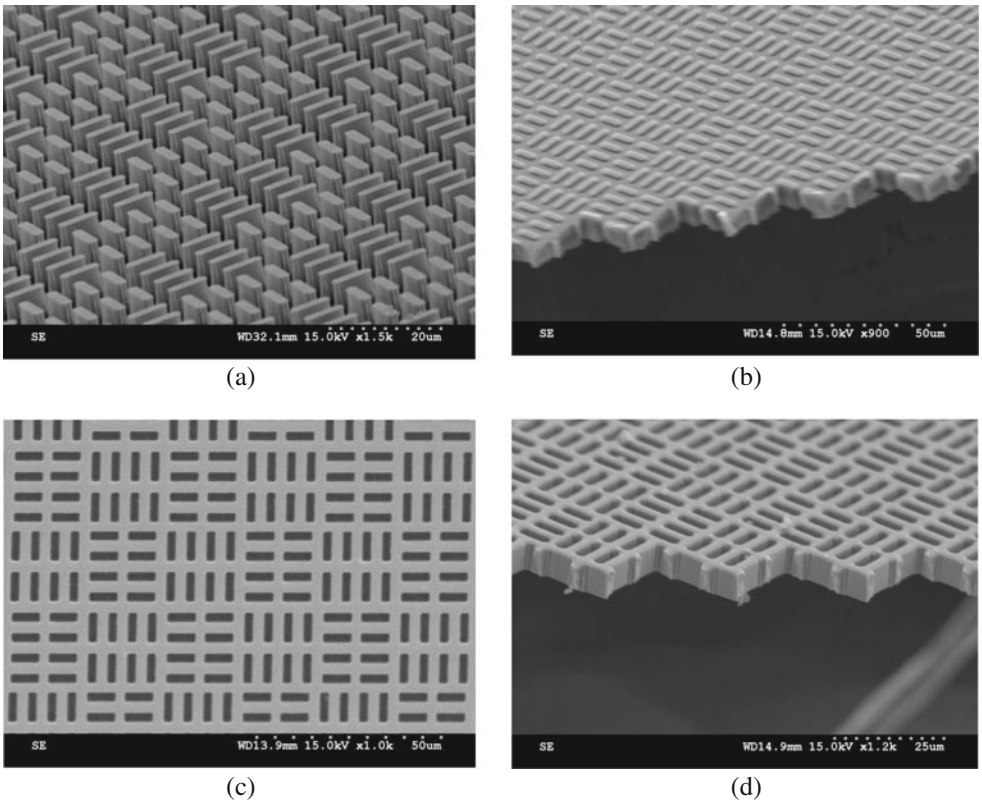

(a) (b) (c) (d)

Fig. 2 (**a**) SEM image of the photo-resist pattern (micro-pillars) used to electroplate the microfilter (**b**) SEM image of a thin Ni layer electroplated between photo-resist pillars, (**c**) SEM image of a through-hole microfilter with slotted pores, and (**d**) cross-section view of the obtained microfilter

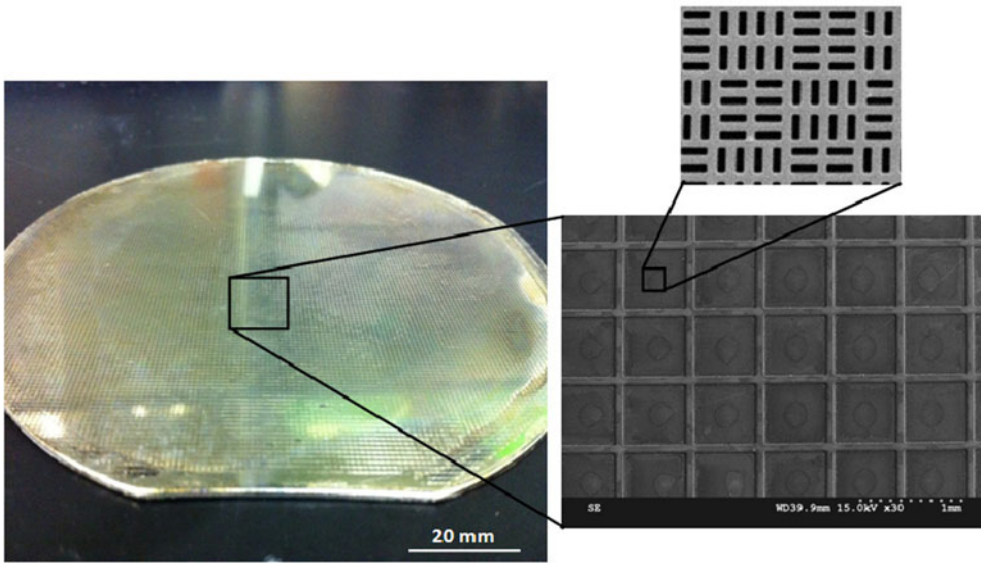

Fig. 3 Optical image of a metallic membrane with integrated back-support before release from the silicon substrate. The SEM images of the integrated back-support and through-hole membrane are also shown in close-ups

For evaluation of the obtained results from the analytical correlation with experimental ones, a small test device similar to the reference (Van Rijn 2004) has been made in which burst pressure of micro-fabricated membranes with different thickness could be measured using a pressure sensor. Figure 4 shows the reciprocal values of bursting pressures for metallic micro-fabricated membranes with square-shaped integrated back-support (600× 600 μm openings) in comparison to the reciprocal values of theoretical bursting pressures calculated using Rijn's model (Van Rijn 2004). The following typical values were used for calculations:

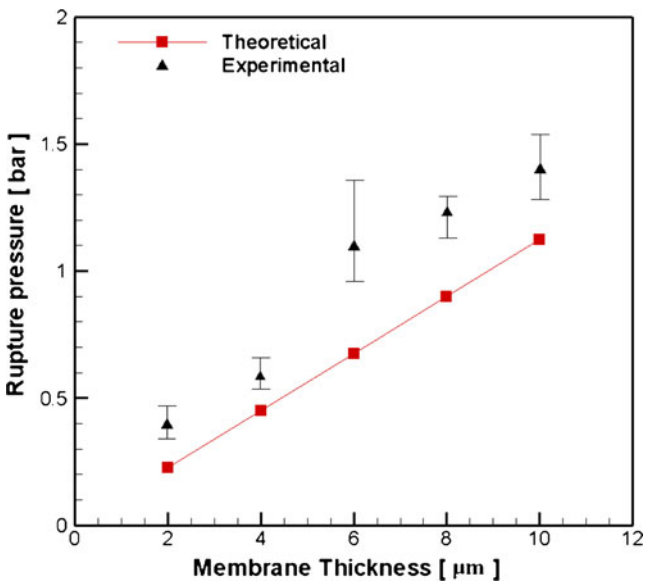

Fig. 4 Reciprocal value of rupture pressure for the metallic micro-fabricated membranes with different thickness in comparison to the theoretical values calculated using Rijn's model

h=2,4,6,8 and 10 μm, l=600 μm, E=210 GPa (Van Rijn et al. 1997), σ_{yeild}=400 MPa (Van Rijn et al. 1997) and K=36 %.

It can be seen that the experimental results for mechanical stability of the micro-fabricated membranes with different thickness are larger than the stability calculated with Rijn's model. This under estimation from this theory is due to the facts that for ductile metals like Ni, Stainless Steel, and Ti, there is a linear relation between the strain and the applied stress up to the yield stress (σ_{yield}). After this point, the membrane may not break and the stress in the middle of the edge (i.e. where the maximum stress is happening) may increase up to the ultimate stress ($\sigma_{ultimate}$). Between the σ_{yield} and $\sigma_{ultimate}$, the membrane strain can increase significantly and E cannot be considered as a constant value (Van Rijn 2004). Therefore, only an under-estimate of the maximum load can be given with above correlation for the ductile materials.

Figure 5 gives an indication of the stress distribution using finite element simulation over the surface of a micro-fabricated membrane with slotted pores. It can be seen that the largest stress is located at the middle of the edges because the total tensile stress at the edge is the summation of the constant tensile stress due to stretching and the bending stress near the middle of the edge (Van Rijn et al. 1997; Kovács et al. 2007). The highest bending stress is also located at the center. From the FEM analyses, it was also found that the deflection of perforated membrane is around 7–9 % larger than for non-perforated membranes for a specified pressure. The aperture size of back-side support has also a large influence on the membrane strength. The FEM results also confirm that the maximum stress is approximately proportional to the applied load and the deflection of membrane at the center is not depending to the

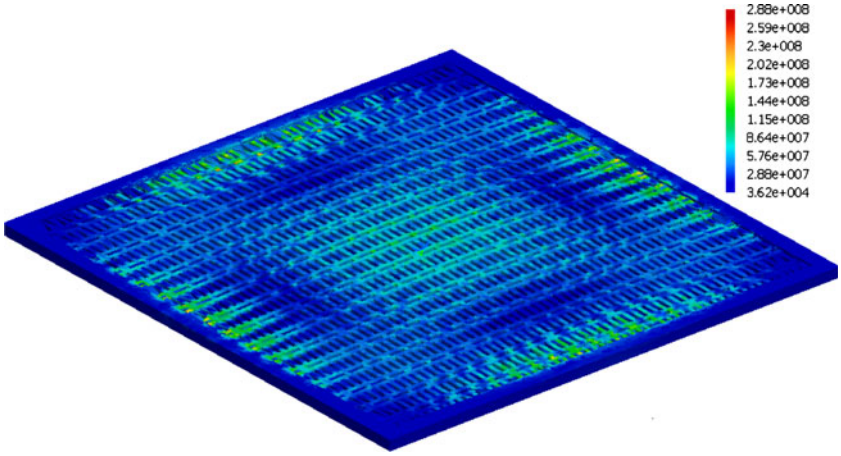

Fig. 5 FEM simulation of the stress distributions over the surface of a perforated membrane with slotted pores, in which only membrane within one support mesh element (600×600 μm) is shown

membrane pore size and thus distribution of the pores (Kovács et al. 2007; Warkiani et al. 2011b).

3.3 Microfiltration with latex particles

Microfiltration with latex particles with specific size can reveal how a pore is blocked and how the performance of a membrane will be with feeds of different particle concentrations. In addition, direct integrity test of the micro-filters before any biological test can be done using appropriate surrogates (like latex particles) by directly assessing the removal of the surrogates (Leonard 2003). Therefore, we evaluate the performance of metallic micro-fabricated filters with slotted pores (2.5×8 μm pore size and 6 μm thickness) using challenge suspensions containing latex particles with 3 μm size. For this purpose, two test solutions with different concentrations (1 g/L and 0.1 g/L) were prepared and filtered through the membranes by a dead-end filtration set up under a constant pressure (0.2 bar). Then, the permeate solutions filtered for the second time through an Anopore™ aluminum membrane (Cat No: 6809–5022) with nominal pore size of 0.2 μm to capture any microbeads that may have passed from the metallic micro-fabricated filter. Subsequently, the surface of aluminum membrane was fully observed under the microscope, and it was realized that no latex particle have been passed through the micro-fabricated microfilter (i.e. 100 % capturing).

Figure 6 shows the obtained result for a slotted pore membrane. It can be seen that severe flux decline occurred with more concentrated feed, producing a permeated volume of around 100 ml. For the diluted feed (0.1 g/L), the flux decline occurred more gradually during filtration.

In order to check the recovery rate of the metallic micro-fabricated filter, its surface was back-flushed (0.2 bar pressure) using a buffer solution containing 0.1 % Tween 80 to remove the beads' layer from the surface of membrane. The results of the optical observation proved that more than 90–95 % of latex particles were recovered. Figure 7 shows SEM photos of the metallic micro-fabricated filter after filtration of latex solution (0.1 g/L) and after back-flushing. Unique features of metallic micro-fabricated filter such as smooth surface and uniform pore-size greatly reduce the latex adhesion to the filter surface and enable us to achieve a very high recovery rate.

3.4 Isolation and recovery of Cryptosporidium parvum oocysts

The performance of the high-flux micro-fabricated microfilter was also assessed by a two-step filtration of *C .parvum* oocysts from tap-water. For comparison, we select two different types of commercially available filters, which were Millipore cellulose acetate membrane (pore size of 1.2 μm, Cat No: RAWP01300) and Envirochek HV filter membrane (pore size

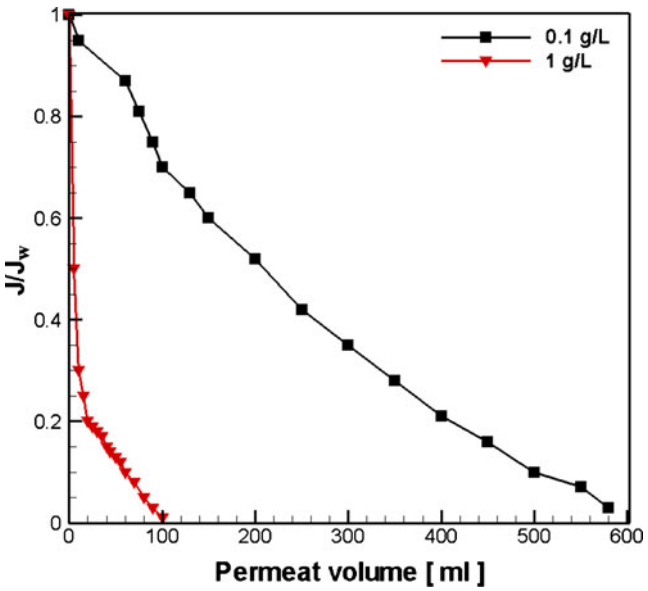

Fig. 6 Normalized flux of two different latex solution concentrations as a function of permeated volume for a slotted pore membrane (2.5×8 μm) with 6 μm thickness

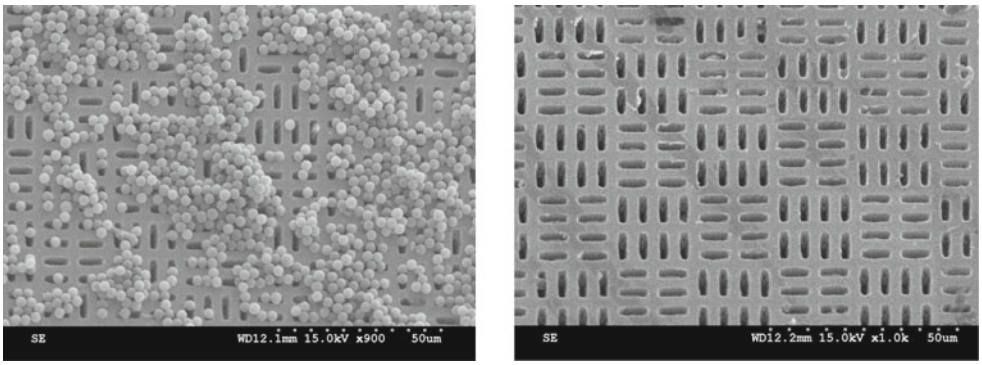

(a) (b)

Fig. 7 SEM images of a metallic micro-fabricated membrane with slotted pores, (**a**) after filtration of latex solution, (**b**) after backflushing with buffer solution

of 1 μm, Cat No: 121110) to evaluate the results substantially. Cellulose acetate membrane is a depth filter, which widely used in industry for fluorescent bacteriological assays, particle monitoring, bioassays and cell separation (Baker 2004; Shepherd and Wyn-Jones 1996). Envirochek HV, a screen type filter, is now serving as the golden standard in concentration of *C. parvum* oocysts from the environmental water samples and is also recommended by USEPA (Clancy et al. 1999).

For this purpose, three similar samples, which was 10 L of tap-water (collected from the tap of our laboratory, turbidity≈ 0.5 NTU, pH=7.6, conductivity=369 μScm^{-1}) inoculated with 2×10^3 heat inactivated *C. parvum* oocysts (Waterborne Inc. New Orleans, LA, USA, Cat No: P102C@1×10^6) with fluorescent tagged antibodies was prepared for the experiments (i.e. according to USEPA methods 1622 and 1623). All the water samples were collected the day of the experiment

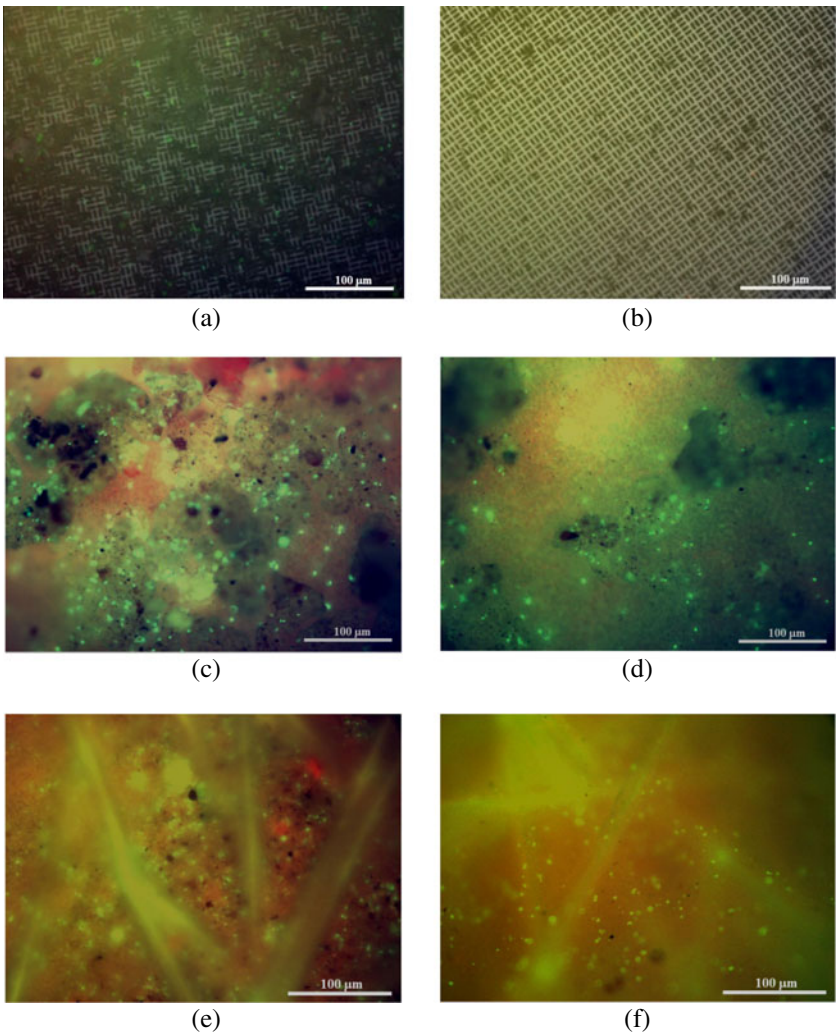

(a) (b) (c) (d) (e) (f)

Fig. 8 Fluorescence microscopic images showing the surfaces of micro-filters after filtration of 10 L of sample (tap-water spiked with 2×10^3 heat inactivated *C. parvum* oocysts) (Left), and after backflushing and lateral shaking (Right), using a Micro-fabricated filter (**a** and **b**), Envirochek filter (**c** and **d**), and Cellulose membrane (a and b)

and turbidity values was measured using an Oakton® T-100 turbidity meter. Membranes were wetted by immersion in ethanol (70 %) for 15 min, and then flushed with DI-water before mounting on the filter holder. The microfiltration was carried out using a peristaltic pump in dead-end mode under 1.5 bar pressure. To assure no oocyst leakage happened from the micro-fabricated microfilter, the filtered sample goes to a subsequent filtration step using an Anodisc filter (Whatman, Cat No: 6809–5522) with nominal pore size of 0.2 μm. Then, surface of both two filters were analyzed under a fluorescence microscope by FITC (fluorescence iso-thiocyanate) technique (Waterborne. Inc., New Orleans, LA, USA, Cat No: A400FLK) to observe the trapped oocysts. Microscopic observations revealed that all oocysts were captured by the micro-fabricated microfilter and no oocyst was found on the Anodisc filter. Then captured oocysts by the microfilters were recovered either by lateral swing, which involved immersing and swinging the filter in water for 5 min, or by back-flush using a 100 ml back-flush buffer solution containing 1 % sodium polyphosphate (NaPP) and 0.1 % Tween 80. The back-flush was performed using the peristaltic pump under 1 bar pressure. The oocysts attached to the microfilters before and after the recovery were visualized by staining the membranes with FITC technique followed by observation under the fluorescence microscope.

The obtained microscopic pictures are depicted in Fig. 8. Careful optical observations of the microfilters revealed that more than 85±7 % of *C .parvum* oocysts were recovered (see Fig. 9) from the micro-fabricated microfilter which appeared significantly higher than the recoveries obtained with Envirochek (55±8 %) or cellulose acetate (30±5 %). Unique characteristics of the metallic micro-fabricated filter like the smooth surface and uniform pore-size greatly reduce the oocyst adhesion to the membrane surface and enable us to achieve a very high recovery rate. For the case of micro-fabricated membrane, the reproducibility of enrichment and recovery was determined for a variety of oocysts' concentrations (i.e. 10^6, 10^5, 10^4 *C. parvum* oocysts spiked in 10 L tap-water), and it was realized that the recovery was around 85±7 % (i.e. a good consistency in recovery rate) according to three individual concentrations enriched in triplicate experiments.

3.5 Flux

Figure 10 depicts the flux of two commercial micro-filters (i.e. track-etched membrane, 2 μm, Millipore and Envirochek HV, 1 μm, Pall) and the micro-fabricated filter under a constant pressure condition using tap-water. The operating pressure was 1.5 bar and the turbidity was around 0.5 NTU. A pressurized container was used to generate constant pressure filtration data. Permeate was collected in a container located on an electronic balance interfaced to a computer.

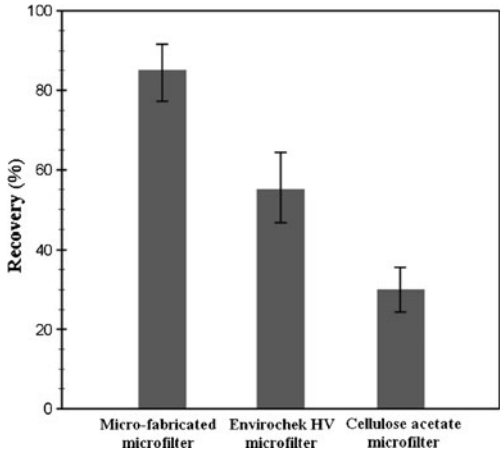

Fig. 9 Recovery of *C .parvum* oocysts from tap-water using Micro-fabricated, Envirocheck and Cellulose microfilters

The microfiltration stand was equipped with a data acquisition unit. The obtained results indicate that the flux of micro-fabricated filter is much higher than two other micro-filters which can be attributed higher porosity and slit shape openings of the micro-fabricated membrane. Experiments were performed in triplicate and presented results are the average of the measurements.

3.6 Other applications

The metallic micro/nano-fabricated membranes have several advantages over existing commercial membranes, which can make them ideal for various applications. In beer industry, they can be used for filtration of yeast because the combination of very smooth surface and low transmembrane pressures

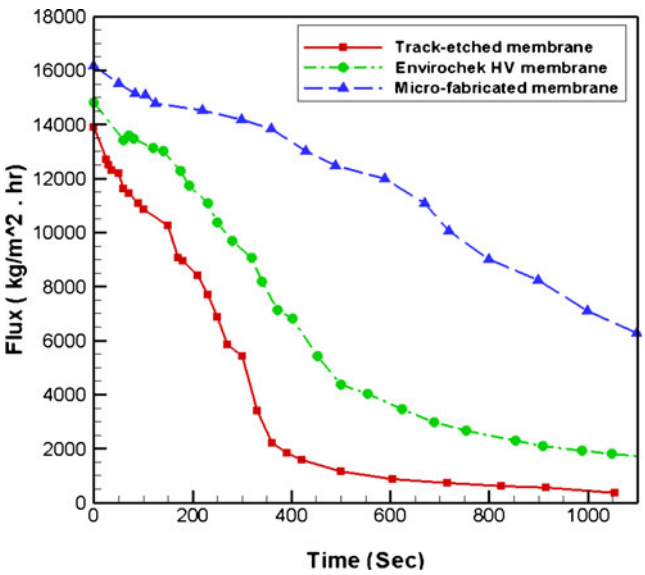

Fig. 10 The flux of two commercial microfilters and micro-fabricated microfilter for filtration of tap-water at a pressure of 1.5 bar and turbidity of 0.5 NTU

makes them less sensible to the protein fouling which is a serious challenge in existing ceramic or polymeric membranes for this purpose. In addition, deposited cake layers can be removed by back flushing and membranes can be cleaned with aggressive chemicals or by steam sterilization. For water monitoring, they can be employed for isolation of waterborne pathogens such as *E-coli*, *Giardia, Salmonella* and *Typhus* in very dilute suspensions to secure the hygiene of drinking water (i.e. section 3.4 proved this hypothesis). Their surface can be coated with bio-compatible materials like Parylene or Heparin (Minteer 2006) to be used for blood filtration, bio-assays and cytology purposes.

4 Conclusions

In this paper, we described a new method for fabrication of high-flux metallic micro/nano-filters with integrated back-support using conventional UV-lithography and electroplating techniques. The present technique is low-cost and high-yield and is capable of fabricating filter membranes having micrometer and potentially nanometer pore sizes. The sieving layer can be made with very small thickness (in order of pore size or even smaller) to present extremely small flow resistance and allows filtration at incredibly low transmembrane pressures. Smooth surface of the membrane reduces the fouling and improve the particles' recovery significantly. This membrane has a long lifetime, and its easy cleanability makes it an interesting choice for large scale applications where conventional membranes need to be replaced most often. This study also highlighted the potential application of micro-fabricated filer in rapid filtration and recovery of *C. parvum* oocysts for downstream detection. In addition, the perfectly defined pores with the slotted shape increase the membrane selectivity and make it suitable for many other applications like blood filtration, microorganism removal, chemotaxis and cytology.

Acknowledgment The authors acknowledge the financial support of the Environment & Water Industry Programme Office of Singapore under the project grant MEWR 651/06/170.

References

F. Ahmad, G. Seyrig, D.M. Tourlousse et al., Biomed. Microdevices, **1** (2011)
R.W. Baker, Membrane Technology and Applications, 2nd Edition, (2004)
N. Beyor, T.S. Seo, P. Liu et al., Biomed. Microdevices **10**, 909 (2008)
M. Chandler, A. Zydney, J. Membr. Sci. **285**, 334 (2006)
L. Chen, M.E. Warkiani, H.B. Liu, H.Q. Gong, J. Micromech. Microeng. **20**, 075005 (2010)
J.L. Clancy, Z. Bukhari, R.M. McCuin, Z. Matheson, C.R. Fricker, J. American Water Works Assoc. **91**, 60 (1999)
M. Gironès, I.J. Akbarsyah, W. Nijdam, C.J.M. van Rijn, H.V. Jansen, R.G.H. Lammertink, M. Wessling, J. Membr. Sci. **283**, 411 (2006)
H. Karim, S. Sylvain, L. Laurence, H. Lucien, C. Henry-Michel, Water Sci. Tech. **62**, 196 (2010)
A. Kovács, Á. Kovács, M. Pogány, U. Mescheder, Sensors Actuators B: Chem. **127**, 120 (2007)
S. Kuiper, C.J.M. Van Rijn, W. Nijdam, M.C. Elwenspoek, J. Membr. Sci. **150**, 1 (1998)
Y. Lee, L. Gomez, I. McAuliffe, V. Tsang, Lett. Appl. Microbiol. **39**, 156 (2004)
B. Leonard, United States, Environmental Protection Agency, Office of Water, (2003)
C.K. Malek, V. Saile, Microelectron. J. **35**, 131 (2004)
J. McGeough, M. Leu, K. Rajurkar, A. De Silva, Q. Liu, CIRP Annals-Manufacturing Tech. **50**, 499 (2001)
S.D. Minteer, Humana Pr Inc. (2006)
E.C. Nieminski, F. Schaefer 3rd, J.E. Ongerth, Appl. Environ. Microbiol. **61**, 1714 (1995)
R.D. Noble, Elsevier science, (1995)
V. Ramachandran, H.S. Fogler, J. Fluid Mech. **385**, 129 (1999)
K. Shepherd, A. Wyn-Jones, Appl. Environ. Microbiol. **62**, 1317 (1996)
P. Spiro, Draper, (1971)
P. Stroeve, N. Ileri, Trends Biotechnol. **29**, 259 (2011)
C. Van Rijn, Elsevier Science, (2004)
C. Van Rijn, M. Van Der Wekken, W. Nijdam, M. Elwenspoek, J. Microelectromech. Syst. **6**, 48 (1997)
M.E. Warkiani, L. Chen, C.P. Lou, H.B. Liu, Z. Rui, H.Q. Gong, J. Membr. Sci. **369**, 560 (2011a)
M.E. Warkiani, C.P. Lou, H.Q. Gong, J. Micromech. Microeng. **21**, 035002 (2011b)
T. Wohlsen, J. Bates, B. Gray, M. Katouli. Appl. Environ. Microbiol. **70**, 2318 (2004)
T. Yanagishita, K. Nishio, H. Masuda, J. Vac. Sci. Technol. B **25**, L35 (2007)
D.S. Zarlenga, J.M. Trout, Vet. Parasitol. **126**, 195 (2004)
L. J. Zeman, A. L. Zydney, CRC, (1996)
M. Zourob, S. Elwary, A. Turner, Springer Verlag, (2008)